NANO LETTERS

2007
Vol. 7, No. 10
3223−3226

Direct Synthesis of Shaped Carbon Nanoparticles with Ordered Cubic Mesostructure

Zhiyong Wang, Fan Li, and Andreas Stein*

Department of Chemistry, University of Minnesota, Minneapolis, Minnesota 55455

Received August 16, 2007

ABSTRACT

Shaped, mesoporous carbon nanoparticles (MSP-3) were prepared in high yield by a simple direct synthesis using a block copolymer surfactant as the mesopore-directing agent and a colloidal crystal to mold the external shape of the particles. The product consisted of monodisperse nanocubes and uniform nanospheres or tetrapods. The nanocubes contained regularly spaced, cagelike mesopores. The orientation of the cubic unit cell describing the mesopore symmetry coincided with the templated external cube faces.

Nanoparticles with well-controlled mesoporosity can provide ready access to a relatively large surface by reducing diffusion lengths compared to bulk materials. As a result, processes that depend on transport of guest species through a porous host can often be enhanced. For this reason, mesoporous nanoparticles have been investigated in the context of a variety of applications such as catalysis and adsorption,[1−3] controlled release of drugs,[4−6] packing for chromatography,[7] and energy storage.[8,9] Here we describe a novel dual-templating synthesis of mesoporous carbon particles, which are amorphous at the atomic level but single crystalline at the mesostructure level. These particles have well-defined cubic external shapes, uniform sizes in the range from 50−150 nm, and ordered arrays of accessible mesopores with cubic symmetry. The cubic particles are mesostructured analogs of much smaller atomic nanoparticles, as they contain only ca. 5−7 unit cells in each dimension. In addition, spheres and tetrapods are produced in this synthesis.

Among the class of mesoporous particles, mesoporous silica spheres have been studied most extensively owing to their well-understood chemistry based on sol−gel processes. Following the pioneering work of aerosol-assisted syntheses of mesostructured silica nanoparticles by Lu and coworkers,[10] a variety of other techniques, including cosurfactant self-assembly,[11,12] phase-separation,[13] and templating with ionic liquids[6] or fluorocarbon-surfactants,[1] were developed for the production of mesoporous silica nanoparticles. Research has also been expanded to mesoporous carbon particles due to their appealing properties such as electrical conductivity and chemical inertness toward most chemicals. These inherent properties open the door to other potential applications such as electrochemical electrodes and energy storage. The most common preparations of mesoporous carbon particles utilize nanocasting strategies that incorporate mesoporous silica nanoparticles as hard templates.[14−17] However, these indirect methods involve laborious synthesis procedures and require the use of environmentally unfavorable reagents such as hydrofluoric acid or strong bases to remove silica templates. To avoid these disadvantages, a one-step synthesis of mesoporous carbon spheres was developed by Zhao's group utilizing an aerosol-assisted self-assembly technique.[18] While this synthesis is fast, it produces carbon spheres with disordered mesopores and a broad particle size distribution from ca. 100 nm to several micrometers. A recent modification of that synthesis led to relatively monodisperse carbon particles with sizes of $\sim$5 μm and ordered mesopore structures with *Im*3*m* symmetry.[19] However, certain applications relying on facile mass transport, for example, fuel cells, would benefit from ordered mesoporous carbon particles with smaller dimensions in the range of ca. 100 nm.[20] Therefore, an efficient, environmentally friendly method for the production of monodisperse, nanometer-sized carbon particles with ordered mesopores is desirable.

Recently a facile method for the preparation of shaped mesoporous silica nanoparticles was discovered by our group.[21] By confining surfactant-templated reactions within a face-centered cubic (fcc) colloidal crystal, uniform silica nanocubes and monodisperse nanospheres or tetrapods are obtained from the disassembly of a 3-D ordered macroporous network. This concept is described in Figure 1. Each unit cell of the fcc colloidal crystal template is composed of four octahedral (O_h) centers and eight tetrahedral (T_d) centers thath are connected by solid bridges. During thermal treatment,

* Corresponding author. E-mail: stein@chem.umn.edu. Telephone: +1-612-624-1802. Fax: +1-612-626-7541.

10.1021/nl072068j CCC: $37.00
Published on Web 09/19/2007

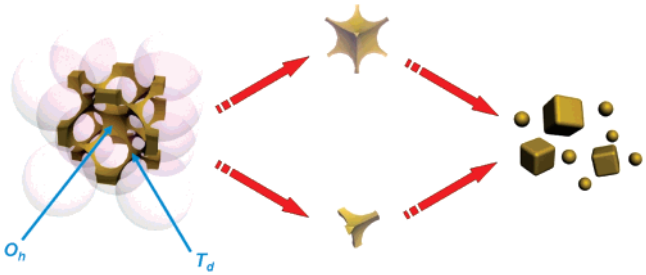

Figure 1. Scheme illustrating the formation of uniform, bimodally dispersed carbon nanoparticles. A PMMA colloidal crystal template (pink spheres) is infiltrated with a precursor solution containing phenolic resin and surfactant. The precursor phase (golden) occupies the void space in the colloidal crystal, which is composed of interconnected octahedral (O_h) and tetrahedral (T_d) centers. During thermal treatments, the connection between O_h and T_d centers breaks, thereby forming discrete cubes with concave faces and tetrapod-shaped particles after the removal of PMMA by pyrolysis. Prolonged heating results in contraction of these primary particles to form nanocubes with rounded corners and spheroids.

the precursor condenses, connections between O_h and T_d centers become thinner, and under the appropriate conditions break to generate discrete nanocubes and tetrapods. Further contraction to minimize surface energies causes rounding of cube corners and the transformation of tetrapods to spherical particles. The edge lengths of the nanocubes and diameters of the spheres are defined by the dimensions of the templating spheres used in the colloidal crystal. Uniform mesoporous carbon nanoparticles can be prepared by nanocasting from these silica nanoparticles via a chemical vapor deposition technique, but because the mesopores in the silica particles are not ordered, those in the carbon replica particles are also disordered.[21] Similarly, mesoporous cubes with disordered mesopores were prepared by a triconstituent synthesis process that required a silica component and etching in hydrofluoric acid.[22] Here we describe a much simpler approach that combines templated disassembly with a direct carbon synthesis to prepare uniformly sized carbon nanocubes with well-ordered mesopores, together with smaller uniform spheres, in a single step.

In a typical synthesis, 2.0 g of phenolic resin solution in ethanol (50 wt %)[23] was mixed with 1.5 g of ethanol and 1.0 g of 0.2 M aqueous hydrochloric acid under magnetic stirring. The acid was found to be vital to ensure complete dissolution of the surfactant during the following step. Next, 0.5−0.7 g of triblock copolymer surfactant, Pluronic F127 ($EO_{97}PO_{69}EO_{97}$, BASF) was added and stirred for 6 h at room temperature to form a homogeneous solution. Monolithic colloidal crystal templates composed of poly(methyl methacrylate) (PMMA) spheres (diameter: 416 ± 11 nm) were infiltrated with this precursor solution at room temperature until the template was fully wetted. Solvents were removed from the precursor-infiltrated monoliths by exposing these to a reduced pressure of ca. 0.5 mmHg for 3 h. The monoliths were then thermally polymerized within a closed container at 100 °C for 48 h. Carbonaceous samples were obtained by heating under flowing nitrogen at 400 °C for 3 h and then at 900 °C for 2 h at a ramping rate of 1 °C min^{-1}. The final product is denoted as MSP-3 (*M*eso*S*tructured *P*articles-3).

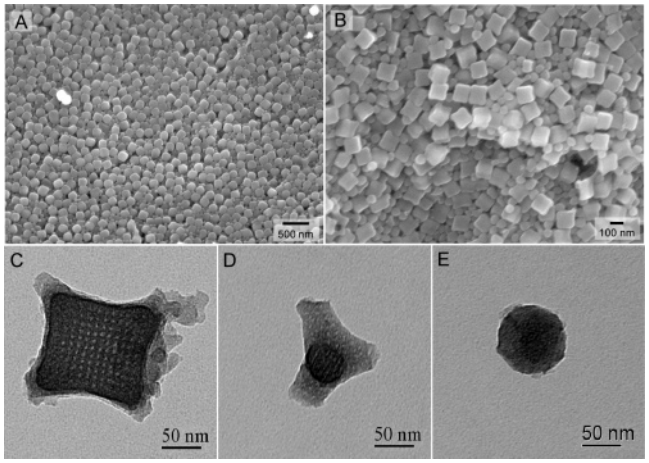

Figure 2. (A,B) SEM images of mesostructured carbon nanoparticles MSP-3. (C−E) TEM images of the mesoporous carbon nanoparticles, (C) cubes, (D) tetrapods, and (E) spheres.

The yield of carbon was 94 wt %, assuming a fully crosslinked phenolic resin as the carbon source.

Scanning electron microscopy (SEM) images of the pyrolized products show nanoparticles with a bimodal size distribution (Figure 2 A,B). Particles with cubic shapes and edge lengths of 150 ± 5 nm, as well as spherical particles with diameters of 67 ± 9 nm, are present throughout most of the sample (85−95%). A small fraction of extraordinary particles consisted of larger pieces composed of incompletely disconnected particles as well as rods or deformed cubes that probably originated from defects in the colloidal crystal template. Within experimental error, the ratio of larger cubes to smaller spheroids is close to the theoretical ratio (1:2) of the numbers of O_h and T_d holes in the face-centered cubic colloidal crystal template; among 2096 particles counted in the SEM image (Figure 2A), 745 cubes and 1351 spheroids are visible, the difference being attributed largely to tetrapodal particles that were observed by transmission electron microscopy (TEM) (Figure 2D) but may be hidden below the visible layers in the SEM image. Many of the cubes originating from O_h interstices have rounded corners (Figure 2B), although in TEM images (Figure 2C), the concave nature inherited from the colloidal crystal mold is visible. The rounded features arise from contraction of solids during thermal treatment as a result of polymerization and carbonization of the phenolic resin and the natural tendency to minimize surface energies during product formation. These processes also caused a transformation of tetrapods from T_d sites (Figure 2D) to mostly spherical carbon particles (Figure 2E). The TEM image (Figure 2C) revealed that many nanocubes are covered with jagged edges, which may be attributed to either fragments from the ruptured bridges or carbonaceous residues from decomposed PMMA.[24]

The carbon nanocubes exhibit ordered mesostructured patterns with cubic symmetry (Figure 2C). The average mesopore diameters estimated from TEM images are ca. 2.4 nm. The cubic mesopore symmetry was confirmed by rotating a single particle during TEM analysis. Images were taken from three viewing directions, [100], [110], and [210]. The observed patterns of pores are similar to those found in

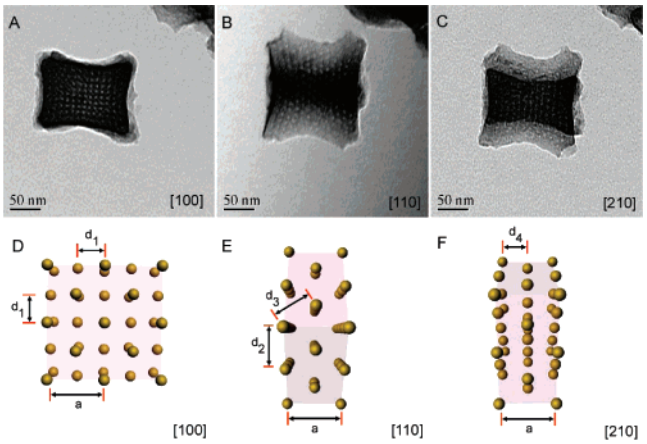

Figure 3. TEM images (A−C) and arrangements of spherical mesopores with fcc symmetry based on the space group *Fm*3*m* (D−F). Here "a" indicates the length of the cubic unit cell and "d_n" (n = 1−4) the characteristic distances between adjacent projections of mesopores. These distances are summarized in Table 1.

Table 1. Measured Characteristic Distances between Adjacent Projections of Mesopores Viewed along Different Axes

axis	distance notation	distance (nm)	length in unit cell	calculated a^a value (nm)
[100]	d_1	9.2	$a/2$	18.5
[110]	d_2	12.2	$a/\sqrt{2}$	17.3
[110]	d_3	11.7	$\sqrt{6}a/4$	19.1
[210]	d_4	9.3	$a/2$	18.6

[a] "a" is the length of one cubic unit cell. See Figure 3 for definitions of the distances d_n (n = 1−4).

published TEM images of materials with fcc mesopores and *Fm*3*m* symmetry,[25] and they could be modeled based on that space group (Figure 3). Characteristic distances between adjacent mesopores measured from the three TEM images (Table 1) indicate an average unit cell length of 18.4 ± 0.8 nm. Interestingly, the orientation of the mesoporous unit cell coincides with that of the carbon nanocube, and at the cube surface, cages follow the surface curvature, suggesting that the packing of micelles is dictated by the colloidal crystal template. In the tetrapodal particles, the mesostructural order could not be established from TEM analysis because of the highly curved surfaces in these particles. Confinement to the narrow dimensions of the tetrapod legs did not permit micelles to form ordered structures in these regions. Similarly, a mesopore structure could not be unambiguously identified by TEM in the nanospheres that originate from the T_d centers (Figure 2D), possibly as a consequence of contraction and densification of the tetrapodal parent structures.

Small-angle X-ray scattering (SAXS) was used to verify the overall mesostructural ordering of the MSP-3 sample (Figure 4A). Because typical cubes contain only ca. 5−7 unit cells in each direction and they are diluted with spheres whose mesostructure is less well defined, the SAXS pattern is weaker than typical SAXS patterns for larger particles. The most intense peak at 0.98° 2θ and two much weaker peaks at 0.83° and 1.39° 2θ can be indexed to the (200), (111), and (220) planes of the fcc lattice, respectively, with

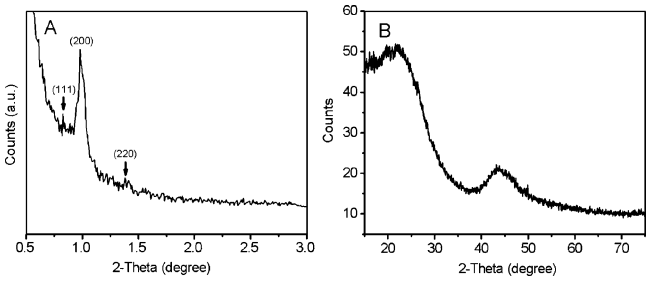

Figure 4. SAXS (A) and powder XRD (B) patterns of MSP-3. Cu Kα sources were used for the SAXS and XRD measurements.

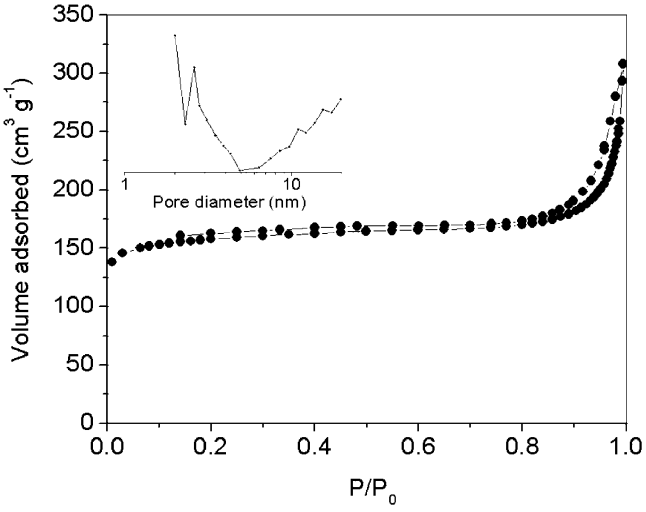

Figure 5. Nitrogen sorption isotherm of carbon nanoparticles. Inset: pore-size distribution curve (adsorption branch) calculated by the BJH method.

a unit cell parameter of a = 18.1 ± 0.3 nm, consistent with the TEM observations. The relative order of peak intensities in these small shaped particles is different from that reported for larger cubic mesoporous particles, where the d_{111} peak is commonly most intense[25−29] but comparable with patterns for highly oriented mesoporous thin films with cubic symmetry in which (200) planes are oriented parallel to the substrate.[30,31] This intensity pattern may be a result of preferred orientation of the uniformly shaped mesoporous particles and therefore of the mesostructured unit cell during SAXS measurements. Such preferred orientation is also apparent in the SEM image (Figure 2A), which shows mostly the (100) faces of the cubes. The carbon walls within each MSP-3 particle are amorphous, as reflected by the two broad peaks at 22° and 43° 2θ in the powder X-ray diffraction (XRD) pattern (Figure 4B).

More detailed information about the porosity of the carbon nanoparticles was obtained by nitrogen sorption measurents. Adsorption and desorption processes follow a type-I isotherm (Figure 5), according to the IUPAC definition,[32] with some type-IV character (two narrow hysteresis loops). This behavior is typically associated with micropores and narrow mesopores. The hysteresis loop between P/P_0 of 0.2−0.6 is attributed to capillary condensation in mesopores; the other loop at higher P/P_0 (0.9−1) may reflect the interparticle texture within the sample. Pore size calculations employing the Barrett−Joyner−Halenda (BJH) method reveal a meso-

pore size peaking at 2.6 nm. This value is close to our TEM estimates but is slightly smaller than that of mesoporous carbon films prepared by an evaporation-induced self-assembly process,[23] which could result from confinement effects in the colloidal crystal and from extensive particle shrinkage. The mesopore wall thickness is 10.4 nm, estimated from the BJH pore size and the TEM-derived unit cell size. The sample has a Brunauer−Emmett−Teller surface area of 532 m^2 g^{-1} and a pore volume of 0.37 cm^3 g^{-1} with a micropore contribution of 54%. The large fraction of micropores is typical for mesoporous carbon materials prepared by poly(ethylene oxide)-based block copolymer surfactants, and the generation of microporosity is explained as the result of the continuous removal of carbon, hydrogen, and oxygen from the thick mesopore walls during carbonization.[33]

In conclusion, we have demonstrated a facile method for the preparation of monodisperse carbon nanoparticles (cubic, tetrapodal, and spherical shapes) via a direct synthesis involving copolymer templating within the confinement of a colloidal crystal. The synthesis avoids the use of hydrofluoric acid and other complications associated with nanocasting methods that have typically been used to prepare mesoporous carbon nanoparticles, and it provides uniform products with high yields. This system provides the first example of highly ordered mesopores with fcc symmetry in nanoparticles prepared by templated disassembly methods. Though the glassy carbon particles are amorphous on the length scale of carbon, they form single crystals at the mesoscale. It is notable that the symmetry axis of the cubic particles and the cubic mesopore arrays coincided, suggesting that the confining environment of the colloidal crystal template influenced the arrangement of the surfactant micelles. We believe that the colloidal crystal template not only shaped the external morphology of the carbon particles but also participated in directing their internal mesostructure through interactions between the surfactant polymer blocks and the PMMA surfaces. On the basis of nitrogen sorption measurements, the whole pore system is accessible to guest molecules and lends itself to a wide range of applications involving host−guest interactions, where guests are separated by predefined distances. A particular advantage of the nanoparticle architectures is that guests are confined in a countable number of cages limited by the 3D volume of the particle. This feature may be useful if guests in specific cages need to be probed because individual cages would be more easily addressable than in larger bulk mesostructures. The cubic particle shape also lends itself to assembly into extended structures.[34]

Acknowledgment. This research was supported by the Petroleum Research Foundation administered by the American Chemical Society (ACS-PRF grant number 42751-AC10), the National Science Foundation (DMR-0704312), the Office of Naval Research (grant number N00014-07-1-0608), and in part by the MRSEC program of the NSF (DMR-0212302), which supports the University of Minnesota Characterization Facility.

References

(1) Han, Y.; Ying, J. Y. *Angew. Chem., Int. Ed.* **2005**, *44*, 288−292.
(2) Tian, R.; Zhang, H.; Ye, M.; Jiang, X.; Hu, L.; Li, X.; Bao, X.; Zou, H. *Angew. Chem., Int. Ed.* **2007**, *46*, 962−965.
(3) Suzuki, K.; Sinha, K. *Chem. Commun.* **2007**, 2547−2551.
(4) Park, C.; Oh, K.; Lee, S. C.; Kim, C. *Angew. Chem., Int. Ed.* **2007**, *46*, 1455−1457.
(5) Kim, H.-J.; Ahn, J.-E.; Haam, S.; Shul, Y.-G.; Song, S.-Y.; Tatsumi, T. *J. Mater. Chem.* **2006**, *16*, 1617−1621.
(6) Trewyn, B. G.; Whitman, C. M.; Lin, V. S.-Y. *Nano Lett.* **2004**, *4*, 2139−2143.
(7) Rebbin, V.; Schmidt, R.; Fröba, M. *Angew. Chem., Int. Ed.* **2006**, *45*, 5210−5214.
(8) Guo, Y.-G.; Hu, Y.-S.; Maier, J. *Chem. Commun.* **2006**, 2783−2785.
(9) Yuan, Z.-Y.; Su, B.-L. *J. Mater. Chem.* **2006**, *16*, 663−677.
(10) Lu, Y.; Fan, H.; Stump, A.; Ward, T. L.; Rieker, T.; Brinker, J. C. *Nature* **1999**, *398*, 223−226.
(11) Suzuki, K.; Ikari, K.; Imai, H. *J. Am. Chem. Soc.* **2004**, *126*, 462−463.
(12) Garcia-Bennett, A. E.; Lund, K.; Terasaki, O. *Angew. Chem., Int. Ed.* **2006**, *45*, 2434−2438.
(13) Rathod, S. B.; Ward, T. L. *J. Mater. Chem.* **2007**, *17*, 2329−2335.
(14) Fuertes, A. B. *J. Mater. Chem.* **2003**, *13*, 3085−3088.
(15) Hampsey, E. J.; Hu, Q.; Rice, L.; Pang, J.; Wu, Z.; Lu, Y. *Chem. Commun.* **2005**, 3606−3608.
(16) Hampsey, E. J.; Hu, Q.; Wu, Z.; Rice, L.; Pang, J.; Lu, Y. *Carbon* **2005**, *43*, 2977−2982.
(17) Ren, J.; Ding, J.; Chan, K.-Y.; Wang, H. *Chem. Mater.* **2007**, *19*, 2786−2795.
(18) Yan, Y.; Zhang, F.; Meng, Y.; Tu, B.; Zhao, D. *Chem. Commun.* **2007**, 2867−2869.
(19) Zhang, F.; Gu, D.; Yu, T.; Zhang, F.; Xie, S.; Zhang, L.; Deng, Y.; Wan, Y.; Tu, B.; Zhao, D. *J. Am. Chem. Soc.* **2007**, *129*, 7746−7747.
(20) Chang, H.; Joo, S. H.; Pak, C. *J. Mater. Chem.* **2007**, *17*, 3078−3088.
(21) Li, F.; Wang, Z.; Stein, A. *Angew. Chem., Int. Ed.* **2007**, *46*, 1885−1888.
(22) Wang, Z.; Stein, A. *Chem. Mater.* **2008**, *20*, http://dx.doi.org/10.1021/cm0717864.
(23) Meng, Y.; Gu, D.; Zhang, F.; Shi, Y.; Yang, H.; Li, Z.; Yu, C.; Tu, B.; Zhao, D. *Angew. Chem., Int. Ed.* **2005**, *44*, 2−8.
(24) Yan, H.; Blanford, C. F.; Stein, A.; Smyrl, W. H. *Chem. Commun.* **2000**, 1477−1478.
(25) Zhou, X.; Qiao, S.; Hao, N.; Wang, X.; Yu, C.; Wang, L.; Zhao, D.; Gao, Q. L. *Chem. Mater.* **2007**, *19*, 1870−1876.
(26) Kleitz, F.; Liu, D.; Anilkumar, G. M.; Park, I.-S.; Solovyov, L. A.; Shmakov, A. N.; Ryoo, R. *J. Phys. Chem. B* **2003**, *107*, 14296−14300.
(27) Matos, J. R.; Kruk, M.; Mercuri, L. P.; Jaroniec, M.; Zhao, L.; Kamiyama, T.; Terasaki, O.; Pinnavaia, T. J.; Liu, Y. *J. Am. Chem. Soc.* **2002**, *125*, 821−829.
(28) Liang, Y.; Hanzlik, M.; Anwander, R. *Chem. Commun.* **2005**, 525−527.
(29) El-Safty, S. A.; Hanaoka, T. *Adv. Mater.* **2003**, *15*, 1893−1899.
(30) Wong, E. M.; Markowitz, M. A.; Qadri, S. B.; Golledge, S. L.; Castner, D. G.; Gaber, B. P. *Langmuir* **2002**, *18*, 972−974.
(31) Zhao, D.; Yang, P.; Melosh, N.; Feng, J.; Chmelka, B. F.; Stucky, G. D. *Adv. Mater.* **1998**, *10*, 1380−1385.
(32) Sing, K. S. W.; Everett, D. H.; Haul, R. A. W.; Moscou, L.; Pierotti, R. A.; Rouquerol, J.; Siemieniewska, T. *Pure. Appl. Chem.* **1985**, *57*, 603−619.
(33) Deng, Y.; Yu, T.; Wan, Y.; Shi, Y.; Meng, Y.; Gu, D.; Zhang, L.; Huang, Y.; Liu, C.; Wu, X.; Zhao, D. *J. Am. Chem. Soc.* **2007**, *129*, 1690−1697.
(34) Li, F.; Delo, S. A.; Stein, A. *Angew. Chem., Int. Ed.* **2007**, *46*, 6666−6669.

NL072068J